# AN INVESTIGATION ON THE MECHANICAL AND TRIBOLOGICAL PROPERTIES OF AN ULTRASONIC-ASSISTED STIR CASTING Al-Cu-Mg MATRIX-BASED COMPOSITE REINFORCED WITH AGRO WASTE ASH PARTICLES

UDC:669-14:539.375.6
Original scientific paper https://doi.org/10.46793/aeletters.2024.9.1.5

**Nagaraju Tenali[1*], G. Ganesan[1], P. Ravindra Babu[2]**

[1]Department of Manufacturing Engineering, Annamalai University, India
[2]Department of Mechanical Engineering, Sheshadri Rao Gudlavalleru Engineering College, India

**Abstract:**
This research work reports the influence of 3-µm-sized Palm Sprout Shell Ash (PSSA) reinforcement on the mechanical and tribological behavior of the Al-Cu-Mg alloy. Composites of varying weight percentages of reinforcement ranging from 1 to 6 at intervals of 1 Wt.% were produced using the ultrasonic-assisted bottom-poured stir casting technique. Microstructural studies, mechanical testing, and wear properties analysis were performed on the alloy and the synthesized composites. The microstructure of the obtained samples was examined using Scanning Electron Microscope, Energy Dispersive Spectroscopy (SEM/EDS), and X-Ray Diffraction (XRD). The XRD patterns provided confirmation of the presence of PSSA ($SiO_2$ and $Al_2O_3$) particles. The addition of PSSA reinforcement has significantly improved the hardness, tensile strength, and compression strength of composites. The hardness, ultimate tensile strength, and compression strength were improved by 13.89%, 24.04%, and 32.93%, respectively, with the 6 Wt.% PSSA-reinforced composite. However, the incorporation of reinforcement has resulted in a decrease in the ductility of the Al-Cu-Mg alloy composite; the maximum decrement of 42.87% was with the 6% PSSA-reinforced composite. Tests were conducted at different loads and speeds to evaluate the wear behavior of the prepared samples. Superior wear resistance was observed in the composites. The fracture and wear mechanisms of reinforced and unreinforced were observed using SEM.

**ARTICLE HISTORY**
Received: 29 January 2024
Revised: 17 March 2024
Accepted: 26 March 2024
Published: 31 March 2024

**KEYWORDS**
Agro waste ash particles, Palm Sprout Shell ash, Metal Matrix Composites, Mechanical Properties, Wear resistance, Fractography, Light weight aluminium based MMCs

## 1. INTRODUCTION

In recent years, a switch from metallic alloys to composite materials has been seen as a result of the increasing need to produce high-quality, high-performance materials. Because of the increase in demand for economical, high-strength, and low-weight materials, aluminium metal matrix composites (AMMCs) represent a front-line advancement in materials science, combining the strength and toughness of metals with the exceptional properties of reinforcement materials. This fusion has led to a class of materials that outperform traditional alloys in critical applications. Basically, AMMCs are a type of composite material that is made up of at least two separate components [1,2]. While the primary component (matrix) must be an aluminum alloy, the second component (reinforcement) may be a different type of metal or an entirely other material, such as a

*CONTACT: Nagaraju Tenali, e-mail: tenali.n1830@gmail.com

ceramic or organic compound [3]. The reinforcing material is often continuous carbon (C), silicon carbide (SiC), boron carbide (B4C), or metal oxide particles such as alumina ($Al_2O_3$) and titanium dioxide ($TiO_2$), and they are inserted into a matrix [4,5]. The introduction of particulate reinforcements can enhance the physio-mechanical properties of composites, enabling them to serve as a substitute for conventional and bulky cast iron and plain carbon steels in automobile applications such as brake rotors and connecting rods [6,7]. The inclusion of these hard ceramic reinforcements in a soft aluminum matrix improves the wear resistance and hardness of the composite. However, the production of hard ceramic particulate reinforcements is not user-friendly, environmentally friendly, or economically viable. In light of these considerations, researchers are exploring alternative cost-effective materials. Argo-waste-based reinforcements offer a readily available solution that is economically feasible while also addressing the growing volume of waste material generated by agricultural activities. Furthermore, they have the potential to contribute to the expansion of the global population and the improvement of living standards [8,9]. Utilizing waste materials may reduce contamination in agricultural fields. Moreover, A biodegradable, inexpensive, low-density composite with desirable mechanical and tribological properties can be produced by AMMCs reinforced with bean pod ash (BPA) [7], rice husk ash (RHA) [10-13], palm oil clinker (POC) and sugarcane bagasse [13], groundnut shell ash (GSA) [14,15], coconut shell ash (CSA) [15,16], melon shell ash (MSA) [17], fly ash, red mud and palm oil fuel ash (POFA). Rice husk ash (RHA) is a more cost-effective reinforcement than conventional ceramic-based reinforcement; it increases the tensile strength and hardness of the composite material Al6061 matrix [18]. Along with mechanical properties, the incorporation of RHA into the AA6061 matrix introduces a nucleation site and results in a more refined grain structure within the aluminum matrix. Additionally, the presence of RHA leads to a reduction in the wear rate of the composites [18-21]. The wear resistance of the Al 7029 alloy can be enhanced by reinforcing it with agricultural waste particles like coconut shell ash (CSA). 7079-aluminum-based composites reinforced with 2% CSA, 3% CSA, and 2% graphite were made by the stir casting method. Both reinforcements are of 60-micron size. Hardness, tensile strength, and wear rate were investigated, and improvements in tensile strength and hardness were observed in both composites in comparison to the base alloy. The specific wear rate is minimal due to the integration of graphite and coconut shell reinforcement; moreover, enhancement in wear resistance was observed heavily due to graphite because it acted as a solid lubricant [21-23]. The mutual effects of stir casting and the double-layer feeding process enhance the tensile strength and hardness of composites due to improved interfacial bonding between the alloy and the nanoparticle reinforcement. Al-Cu-Mg reinforced with nano-sized particulate bean pod ash (BPA) made by the process with varied compositions of 1–4 Wt.% were investigated. It is observed that the density of the composite is inversely proportional to the reinforcement percentage. An improvement of 35% in tensile strength and 44% in hardness was observed at 4% reinforced composite. The impact strength and ductility of composites are reduced slightly [24]. The research findings indicate that the utilization of agricultural waste as reinforcements in composites does not result in the formation of brittle materials; considerable promise as a viable alternative to costly and environmentally hazardous conventional ceramic-reinforced composites, these ceramic-reinforced composites can be particularly advantageous in various automotive applications that necessitate a higher strength-to-weight ratio, lower expenses, and superior resistance to wear [25]. Hence, the main objective of this investigation is to study the mechanical and tribological properties of the base material through the incorporation of micro-sized palm sprout shell ash particles using the ultrasonic-assisted bottom-poured stir casting technique. The wear resistance, density, hardness, impact strength, tensile strength, and compression strength of the metal matrix composites are thoroughly investigated and compared to those of the Al-Cu-Mg alloy.

## 2. MATERIALS AND METHODOLOGY

### 2.1 Synthesis of Al-Cu-Mg Alloy

The Al-Cu-Mg was used as the matrix material for this investigation. The stir-casting process prepared alloy, and Al2024 and Al6061 were used as raw materials. Commercially available Al2024 and Al6061 alloys were obtained in rod form (Fig. 1) from Krish MET Tech Limited, Chennai. The chemical composition of the alloys is presented in Tables 1 and 2. The Al-Cu-Mg matrix material was fabricated by combining 75 Wt.% of Al2024 alloy and 25 Wt.% of Al 6061 alloy. The mixture was

loaded into a zirconia-precoated stir-casting furnace mold and heated to a temperature of 750°C. The slag was carefully removed from the melt, and a $Cl_2Cl_6$ degassing agent was added. To ensure a homogeneous distribution of elements, the melt was mechanically stirred using a zirconia-precoated stainless-steel stirrer operated by a motor. The stirring process was conducted with an average speed of 350 rpm for approximately 3 minutes, followed by an average speed of 450 rpm for another 3 minutes. Subsequently, the molten alloy was poured into a preheated mold, which was maintained at a temperature of 300°C for approximately 30 minutes to facilitate uniform solidification. After cooling to room temperature, the resulting casting was obtained. (Fig. 2). In order to prevent oxidation, a shielding of argon gas is maintained over the molten material throughout the entire production process.


**Fig. 1.** Obtained Al2024 and Al 6061 alloys

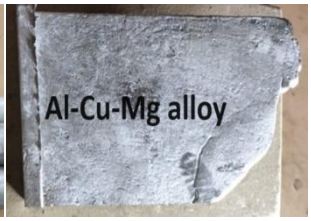


**Fig. 2**. Fabricated Al-Cu-Mg alloy

**Table 1.** Chemical elements presented in the Al2024 alloy

| Elements | Cu | Mg | Si | Zn | Fe | Cr | Ti | Al |
|---|---|---|---|---|---|---|---|---|
| Wt. % | 3.8-4.9 | 1.4-1.8 | 0.5 | 0.25 | 0.5 | 0.1 | 0.06 | Balance |

**Table 2.** Chemical elements presented in the Al6061 alloy

| Elements | Si | Cu | Zn | Fe | Mn | Mg | Cr | Ti | Al |
|---|---|---|---|---|---|---|---|---|---|
| Wt.% | 0.04-0.08 | 0.1-0.4 | 0.09 | 0.07 | 0.15 | 1.8 | 0.04-0.35 | 0.15 | Balance |

Further, an energy-dispersive X-ray spectrometer (EDX) analysis was performed on the matrix material to determine the chemical elements present in it and their respective compositions. The analysis was carried out using the JCM 6000 Plus instrument, which operates within an energy range of 0–20 KeV with an average voltage of 15.0 kV and a probe current of 1.0000 nA. In Fig. 3, the Energy Dispersive X-ray Spectrometer of Al-Cu-Mg alloys (the matrix material) is depicted, while Table 3 provides information on the chemical elements found in the matrix. Further X-ray diffraction analysis (XRD) was conducted to determine the crystallographic structure of the matrix material. The investigation was performed using a RIGAKU Smart Lab XRD instrument with Cu Kα radiation.

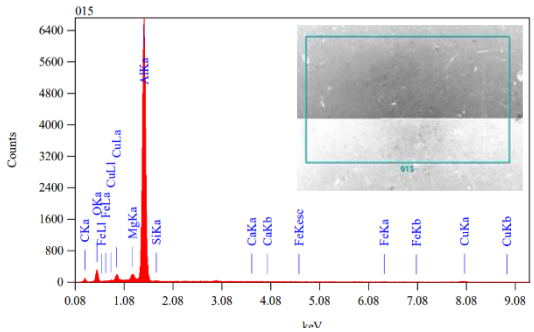


**Fig. 3.** X- ray diffraction analysis of Al-Cu-Mg alloys

The 2θ range was carefully chosen to encompass all the prominent peaks corresponding to the material's predictable phases. Fig. 4 illustrates the XRD pattern obtained for the Al-Cu-Mg alloy.

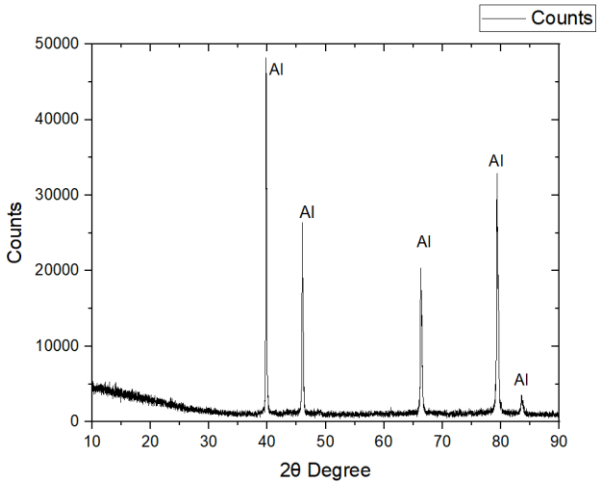


**Fig. 4**. X-ray diffraction patterns of Al-Cu-Mg alloy

**Table 3.** Chemistry of prepared Al-Cu-Mg aluminium alloy

| Element | Cu | Mg | Si | Ca | C | Fe | Al |
|---|---|---|---|---|---|---|---|
| Wt.% | 3.48 | 1.73 | 0.16 | 0.08 | 0.80 | 0.37 | Balance |

## 2.2 Synthesis of Reinforcement

Palm sprout shell ash (PSSA) is the reinforcement for this research. The palm sprout

shells were collected from the fields of K-rishna, coastal Andhra Pradesh, India. They were cleaned with fresh water and dried for ten days in a normal, open, and dry environment. The dried sample was calcined in a closed environment around 700 °C for 4 to 5 hours in an electric arc furnace. Further, the size of the powder particle was reduced during the dry ball milling process. A planetary mill with a tungsten carbide ball is used in this work, and particle size analysis has been conducted using the Laser Scattering Particle Size Distribution Analyzer LA-960. The mean size was identified as 3.43553 (µm), median size 1.07697 (µm), and St. Dev. 7.1081 (µm), depicted in Fig. 5. Both were done at the V.B. Ceramic Research Centre in Chennai.

Further ash was decarburized in a muffle furnace for 3 hours at 250 °C. SEM/EDX microscopy was conducted on ash. Fig. 6 shows the SEM micrograph of ash, showing the microparticles agglomerated Irregular polygonal and spherical shapes, Table 4 shows the chemistry of Plam Sprout shell ash obtained from EDX.

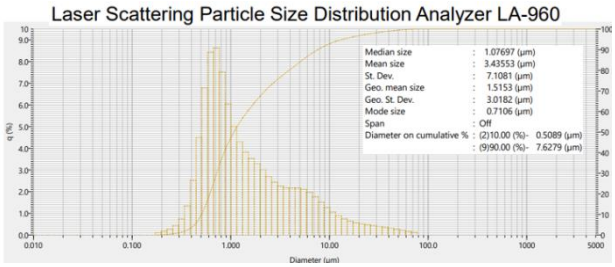


**Fig. 5.** Particle size analysis of Palm sprout shell ash

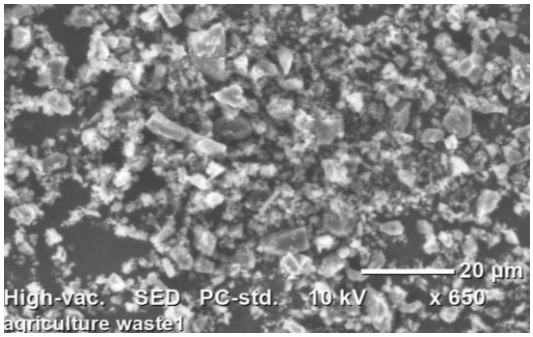


**Fig. 6.** SEM micrographs of PSSA

**Table 4.** Chemistry of Palm Sprout shell ash

| Element | $SiO_2$ | $Al_2O_3$ | CaO | C | $Fe_2O_3$ | ZnCl | $P_2O_5$ | $Na_2O$ | $K_2O$ | $SO_3$ |
|---|---|---|---|---|---|---|---|---|---|---|
| Wt.% | 45.92 | 37.78 | 2.92 | 2.1 | 2.29 | 2.1 | 4.12 | 1.2 | 0.77 | 0.80 |

### 2.3 Fabrication of Composites

In this work, ultrasonic-assisted bottom pour stir casting equipment (shown in Fig. 7) was used to produce the composites. Initially, the mold and stirrer were precoated with zirconia. Al-Cu-Mg alloy plates were made into small pieces. The predetermined quantity of aluminium matrix material pieces (as indicated in Table 5) was introduced into the furnace and heated up to 700 °C. Concurrently, the reinforcement material was heated to 250 °C using a muffle furnace. The PSSA is quite light in weight, so it can be incorporated into the matrix by shaping it into small spheres. Each reinforcement unit weighing 4 gm was made into a sphere by covering it with a thin aluminium sheet before preheating. As the alloy transitioned into a state of melt, slag was removed. Hexa-chloroethene ($C_2Cl_6$) was added to the melt; it acts as a degassifier [26-28]. Further, the melt was cooled to 500 °C in the furnace itself. Subsequently, the preheated microparticle reinforcement balls were added to the melt at the required weight percentages and manually stirred until fully mixed [29]. To maintain wettability, approximately one weight percent of Manganese was included in the molten mixture. The melt was heated up to 750 °C and subsequently stirred mechanically by a motor-operated stainless-steel stirrer. The stirring process was prudently continued to ensure a homogeneous distribution, with an average stirring speed of 400 rpm for approximately 5 minutes [29,30]. Further, an ultrasonic stirrer (sonicator) was carefully induced in the melt blend for around 5 minutes. Ultrasonic vibrations have the capability to disintegrate clusters or agglomerates of reinforcing particles smallest in size, aiding in the even dispersion of these microparticle particles within the molten metal matrix. Consequently, this promotes enhanced homogeneity and distribution of the reinforcement in the composite. Furthermore, it facilitates superior wetting and bonding between the reinforcing particles and the metal matrix, ultimately resulting in a more robust interface between the two phases [31]. The high-intensity ultrasonic generator, operating at an input frequency of 20 kHz and an input power of 20 kW, facilitated the stirring process by generating high-frequency ultrasonic sound waves [32]. The melt was ultimately poured into a mold that had been preheated to a temperature of 300 °C for approximately 30 minutes, ensuring a consistent

solidification process. Afterward, the casting was allowed to cool down to room temperature. Fig. 8 displays a sample of the Al-Cu-Mg-PSSA composite obtained through this procedure. Subsequently, the castings underwent a homogenization process in a muffle furnace, where they were heated up to 250 °C. This step aimed to alleviate any internal stress that may have arisen during the casting process [33]. The same procedure was repeated to prepare all seven castings, as mentioned in Table 5. The castings were machined, and specimens were prepared as per ASTM and tested for density, hardness, impact strength, tensile strength, compression strength, microstructure analysis, and wear analysis.

**Fig. 7.** Ultrasonic-assisted bottom-poured stir-casting machine

**Table 5.** Composites: Reinforcement and matrix proportions

| Sample type | As cast | C1 | C2 | C3 | C4 | C5 | C6 |
|---|---|---|---|---|---|---|---|
| Reinforcement (Wt.%) | 0 | 1 | 2 | 3 | 4 | 5 | 6 |
| Matrix Metal (Wt.%) | 100 | 99 | 98 | 97 | 96 | 95 | 94 |
| Total | 100 | 100 | 100 | 100 | 100 | 100 | 100 |

**Fig. 8.** Prepared Al-Cu-Mg and PSSA composite casting

### 2.4 Microstructural Characterization

Microstructural characterization was performed on samples of both unreinforced and reinforced composites. The specimens were prepared as per the standard of metallography: the specimens were mounted in Bakelite and polished on a series of abrasive (SiC) emery papers of increasingly finer grit sizes (200, 320, 400, 600, and 800) and using alumina powder of 1µm size with a special polishing cloth on a double disc polishing machine. The samples underwent chemical etching by immersing them in Keller's reagent, which consisted of 5 ml of nitric acid, 2 ml of hydrofluoric acid, 3 ml of hydrochloric acid, and 190 ml of distilled water. The etching process lasted approximately 15 to 30 seconds. Subsequently, the samples were rinsed with running water and dried thoroughly. Samples were observed using a computerized optical metallurgical microscope with image analysis software. Surface morphology was conducted through Scanning Electron Microscope- SEM/EDS (JEOL JSM-6380LA) and X-ray diffraction. These analyses were conducted on both alloys and composites.

### 2.5 Evaluation of Mechanical Properties

For this work, the mechanical properties under investigation were tensile strength, compression strength, impact strength, and hardness. The examinations were conducted as per ASTM. The tensile strength and Compression Strength of composites were measured using the electronic model UTE-40. Universal testing machine (UTM) tests were conducted using ASTM E8 and ASTM E9, respectively. For each examination, three tests were conducted on three samples, and the average values of the tested three were computed. One of the tested samples set passed the tensile test and compression test, as shown in Fig. 9 a) and b), respectively. Charpy impact testing machine and ASTM E23 were used to conduct impact tests. The standard square impact test sample measured 55x10x10 mm with a 2mm depth V-notch in the middle. Three samples were tested, and the average values of the three tested were computed. The hardness of castings was measured by a Vickers hardness tester (LECOAT700 Microhardness Tester) as per ASTM E384. During testing, a load of 100 gm. was applied to the specimen for 10 seconds through a square-based diamond indenter. Three trials were conducted on each sample.

a)

b)

**Fig.9.** Al-Cu-Mg added 3% PSSA Composite tested sample: a) tensile test; b) compression test

### 2.6 Evaluation of Density

The composites' densities were determined through both theoretical and experimental methods. The experimental density was measured utilizing the Archimedes principle [3], while the theoretical density was calculated using the rule of mixture. Further, the percentage porosity of the specimens was calculated using the following equation (1) [34] (the values were tabulated in Table 6).

$$\%\, porosity\ = \frac{\rho_T - \rho_{\exp}}{\rho_T} \times 100 \qquad (1)$$

Where are:

$\rho_T$ - Theoretical density and

$\rho_{exp}$ - Experimental density.

**Table 6.** Densities and expected porosities

| Composite Sample type | Theoretical Density g/cc | Experimental Density g/cc | % Porosity |
|---|---|---|---|
| As cast | 2.74 | 2.73 | 0.36 |
| C1 | 2.68 | 2.665 | 0.56 |
| C2 | 2.63 | 2.615 | 0.57 |
| C3 | 2.57 | 2.552 | 0.7 |
| C4 | 2.51 | 2.487 | 0.92 |
| C5 | 2.46 | 2.438 | 0.89 |
| C6 | 2.42 | 2.397 | 0.95 |

### 2.7 Evaluation of Tribological Properties

Upon analyzing the mechanical properties acquired, it is evident that these composites have the potential to be utilized in IC engine parts, specifically connecting rods [23,24]. The large and small ends of the rod are designed to function as bearings. With respect to the operating conditions of a 135cc engine, the average sliding distance is approximately 3768 m at a velocity of 2.15 m/s. the behavior of unreinforced and reinforced composites of Al-Cu-Mg and PSSA was analyzed behavior of unreinforced and reinforced composites of Al-Cu-Mg and PSSA was analyzed by a pin-on-disc dry wear apparatus (DUCOM TR201 with data acquisition software) at room temperature. The test was conducted according to the ASTM G99-05 standard, and a cylindrical pin with a diameter of 8mm and a length of 30 mm was prepared [35,36]. The test conditions were selected based on relevant literature, with the most significant parameters being Load (N), Sliding velocity (m/s), and Sliding distance (m) [36-38]. The wear was measured in the wake of guiding the dry sliding on an EN 31 steel disc and wear tests with loads of 10, 30, 50, and 70 N at 3.14 m/s sliding velocity. The pin was subjected to a sliding distance of 3768 m. In a similar way, wear is conducted on all Al-Cu-Mg and PSSA composites, which were examined at different sliding velocities of 0.88 m/s, 1.88 m/s, 2.51 m/s, and 3.14 m/s at 70 N load and 3768 m sliding distance.

## 3. RESULTS AND DISCUSSIONS

### 3.1 Microstructural Analysis

The optical microstructural images of the Al-Cu-Mg alloy with different weight percentages (1, 2, 3, 4, 5, and 6 Wt.%) of PSSA particles are represented by Fig. 10 a)–f) and Fig. 11 displays the image of the as-cast alloy. The figures illustrate clear grains and grain boundaries, as well as free voids and other casting defects. Analysis of the micrographs reveals the presence of microparticles in the PSSA-reinforced composites, which are clearly visible. The black regions within the structure correspond to the PSSA particles, while the fair regions indicate the presence of aluminium. Importantly, these particles are uniformly dispersed without any clustering or agglomeration. A similar finding was made by Ajagol et al. [39].

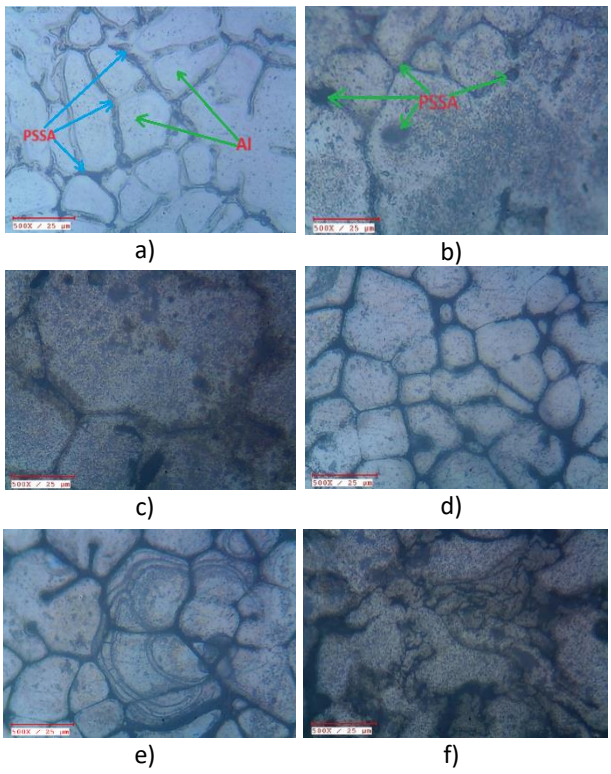


**Fig. 10.** Microscopic images: a) Sample C1 at 500X Magnification; b) Sample C2 at 500X Magnification; c) Sample C3 at 500X magnification; d) Sample C4 at 500X Magnification; e) Sample C5 at 500X Magnification; f) Sample C6 at 500X Magnification

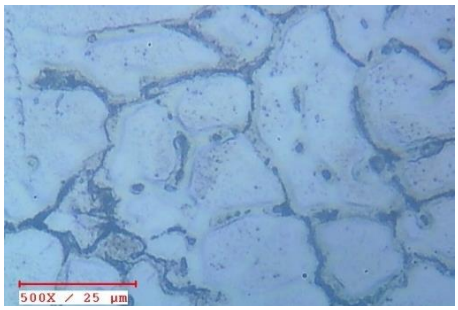


**Fig. 11**. Optical Microstructural image of Al-Cu-Mg alloy

Further examination of the microparticles' structural morphology was conducted through Scanning Electron Microscope (SEM) along with EDS and XRD. The SEM images presented in Fig. 12 and Fig. 13 a) are of 1 Wt.% and 6 Wt.% reinforced composites, respectively. The SEM analysis reveals the 3-µm-sized PSSA particles presented in irregular polygonal shapes, along with a few spherical shapes with uniform distribution. Whereas Fig. 13 b) illustrates the interference between alloy and reinforcement, it is evident that the non-reactive interfacial bonding between reinforcement and Al-Cu-Mg alloy is evident.

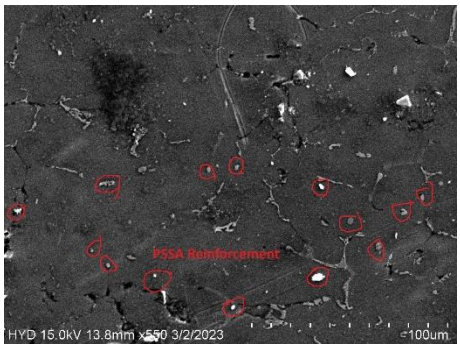


**Fig. 12.** SEM morphology of Al-Cu-Mg added with 1%Palm Sprout Shell Ash (PSSA)

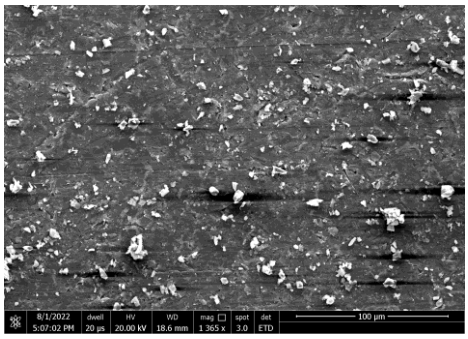


a)

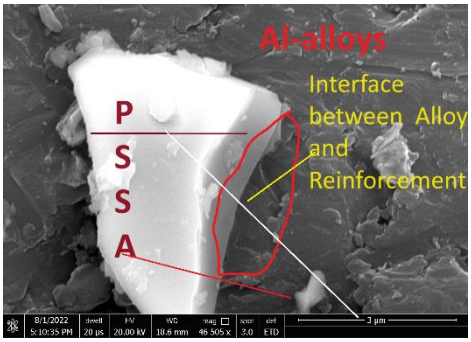


b)

**Fig. 13.** a) SEM morphology of Al-Cu-Mg added with 6%Palm Sprout Shell Ash (PSSA) at 1000X; b) SEM morphology (interface between alloy and PSSA) of Al-Cu-Mg added with 6%Palm Sprout Shell Ash (PSSA) at 46505X

Further energy-dispersive spectra (shown in Figs. 14 and 15) of composites show the presence of PSSA reinforcement in the form of C, Si, Ca, Mn, k, O, and Na. Fig. 4 and Fig. 16 indicate the X-ray diffraction pattern of the Al-Cu-Mg alloy and its composite reinforced with 6 Wt.% of PSSA, respectively. The figures demonstrate phases present in samples. In the X-ray diffraction (XRD) pattern of the Al-Cu-Mg alloy (Fig. 4), the presence of aluminum phases can be observed at various peaks. Specifically, aluminum phases have been confirmed at 38°81', 46°02', 66°03', 79°38', and 88°9', exhibiting different intensities. Notably, the peak at 38°81' exhibits the highest intensity among

all the aluminum phases. When examining the Al-Cu-Mg alloy with the addition of 6% PSSA particles (Fig. 16), the same peaks for aluminum alloy phases are observed. However, in addition to these peaks, multiple peaks have been identified for the PSSA ($SiO_2$ and $Al2O_3$) particle phases at various 2θ angles, each with varying intensities. The $SiO_2$ phase peaks have been found at angles 20°05', 27°08', 36°96', 38°67', 50°16', 60°25', and 67°91'. On the other hand, the $Al_2O_3$ phase peaks have been found at angles 25°02', 35°01', 39°27', 44°03', 53°05', 58°01', and 77°7'. Consequently, the X-ray diffraction pattern has provided evidence that the composites indeed do incorporate PSSA reinforcement.

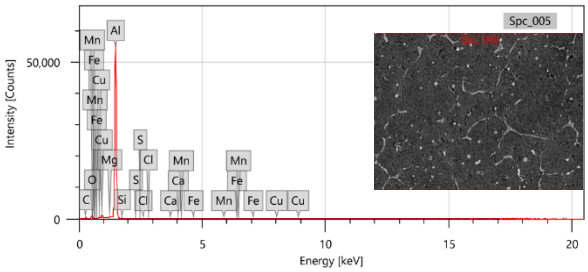


**Fig. 14.** EDS spectrum of Al-Cu-Mg added with 1% Palm Sprout Shell Ash (PSSA)

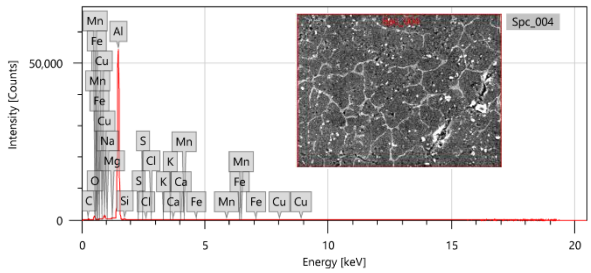


**Fig. 15.** EDS spectrum of Al-Cu-Mg added with 6% Palm Sprout Shell Ash (PSSA)

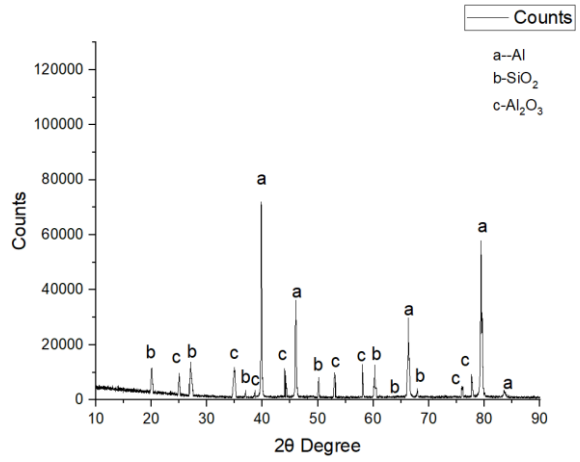


**Fig. 16.** X-ray diffraction patterns of Al-Cu-Mg added 6 Wt.% PSSA composite

### 3.2 Density of Composites

The densities of the Al-Cu-Mg alloy and its composite reinforced with PSSA microparticles (weight percentages 1-6) are presented in Fig. 17 a). The theoretical densities were calculated based on the rule of mixtures of composites. Further experimental densities were measured: the density of the Al-Cu-Mg alloy was 2.74 g/cm$^3$, and the PSSA was 0.84 g/cm$^3$. In Fig. 17 a), it can be observed that the density of the material decreased as the weight percentage of PSSA increased from 1 to 6. The density values decreased from 2.665 g/cm$^3$ to 2.397 g/cm$^3$. This reduction in density can be attributed to the incorporation of PSSA particles, which have a lower density compared to the Al-Cu-Mg matrix. The decreased density of the reinforced particles results in a decrease in the overall composite density.

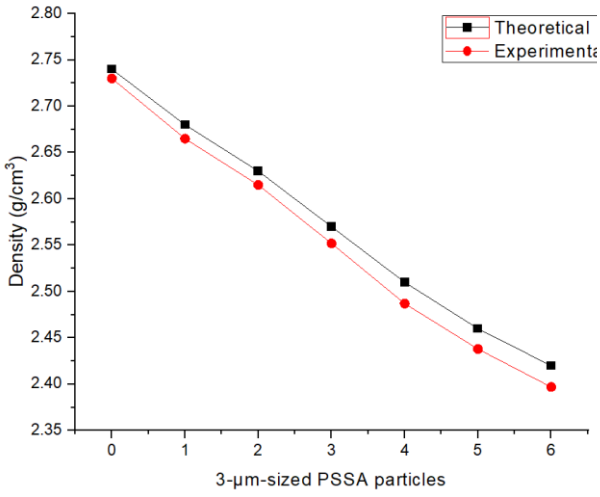


a)

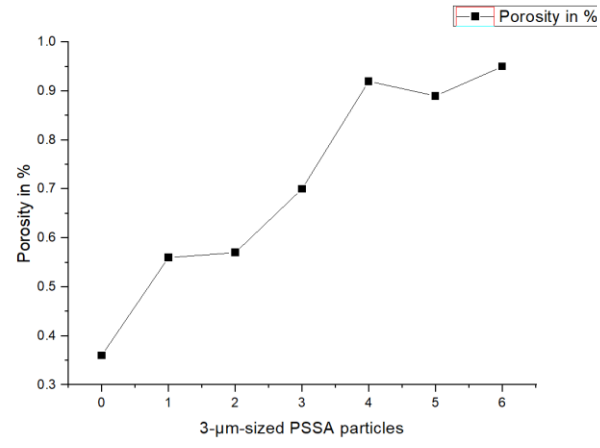


b)

**Fig. 17.** a) variation in density; b) variation in % Porosity of the AL-Cu-Mg alloy added with PSSA

Furthermore, as shown in Fig. 17 a), the experimental density is slightly below the

theoretical density. The difference between the theoretical density and the experimental density is very small. For example, the 1 Wt.% PSSA reinforced composite theoretical density is 2.68 g/cm$^3$, and the experimental density is 2.665 g/cm$^3$. As the percentage of reinforcement increased from 0% to 6%, the percentage of porosity increased from 0.36 to 0.95%. This shows (Fig. 17 b) that the addition of reinforcement may be the reason for the occurrence of porosity, which in turn lowers the density of composites [40,41]. This highlights the importance of the ultrasonic-assisted stir-casting method used to prepare the composite matrix.

### 3.3 Tensile Strength

The impact of incorporating 3-µm-sized PSSA particles on the tensile behaviour (Ultimate stress vs strain) of alloy and composite, illustrated in Figs. 18 and 19, shows a variation of reinforcement effect on the ultimate tensile strength of the Al-Cu-Mg alloy.

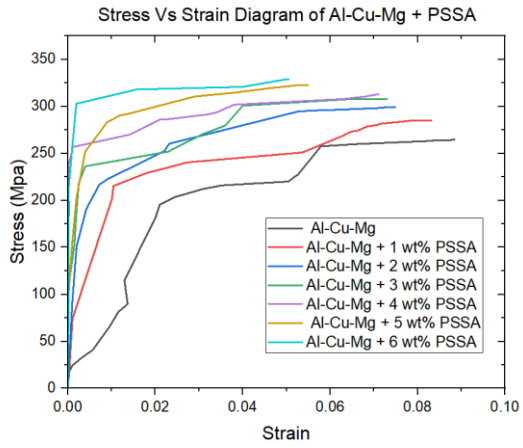


**Fig. 18.** Stress and Strain diagrams of the alloy and composites

The inclusion of PSSA particles has resulted in an improvement in the tensile strength of the Al-Cu-Mg alloy. The ultimate tensile strength of the Al-Cu-Mg alloy measures 265 N/mm$^2$, and when reinforced with 6 Wt.% of PSSA particle composites, the ultimate strength reaches 328.7 N/mm$^2$. Notably, the strength of the alloy exhibits a relative increase as the weight percentage of PSSA in the alloy progresses from 1 to 6 Wt.%. Further. The presence of 3-µm-sized PSSA particles plays a crucial role in improving the strength of the base alloy. The rise in the tensile strength of the Al-Cu-Mg composite is a result of the coefficient of thermal expansion mismatch between PSSA (ceramic) and the aluminium alloy. This mismatch induces strain, which acts as a prestress on the matrix. Furthermore, it can also release dislocation loops and mitigate thermal stress. Consequently, the incorporation of ceramic particles results in a higher dislocation density within the lattice material, thereby enhancing the strength of the aluminium network [24,36].

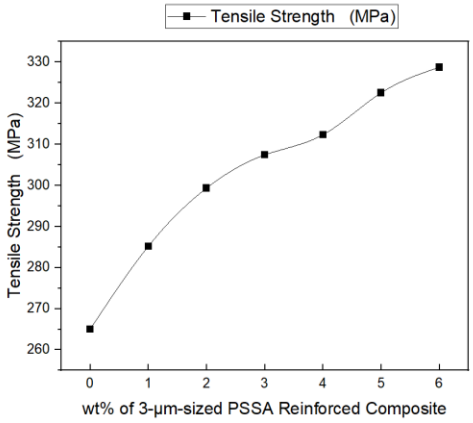


**Fig. 19**. Effect of reinforcement on Ultimate Tensile strength Al-Cu-Mg alloy composites

### 3.4 Percentage of Elongation

The impact of 3-µm-sized PSSA particles on the ductile behavior of the Al-Cu-Mg alloy is illustrated in Fig. 20. The addition of PSSA particles leads to a reduction in the ductility of the fabricated composites. This decrease in ductility can be attributed to the inclusion of rigid PSSA particles. As the weight percentage of PSSA increases from 1 to 6 Wt.%, the ductility experiences further deterioration. These particles act as a constraint on the deformation of the Al-Cu-Mg alloy matrix due to the presence of PSSA. The comparison of tensile strength ductility of the composites is illustrated in Fig. 21. The graph demonstrates that the tensile strength experiences a proportional increase as the weight percentage of reinforcement increases. In contrast, the ductility shows an inverse relationship, decreasing as the weight percentage of reinforcement rises. The decrement of ductility and improvement of tensile strength follow almost the same proportionate Up to 3% PSSA reinforcement. Further, a rise in % of PSSA effect more decrement in ductility in comparison to the increment in tensile strength. The decrease in ductility can be attributed to the incorporation of rigid ceramic PSSA particles within the soft and ductile aluminium matrix (tensile fracture of alloy depicted in Fig. 22), resulting in a decline in elastic properties. This phenomenon is more pronounced with an increase in the percentage of inclusions, as evidenced by the composite reinforced with 5 Wt.% and 6 Wt.%. Fig.

23 depicts this phenomenon, showing that more brittle fractures were observed in Fig. 23 c) compared to the previous Figs. 23 a) and b). A similar phenomenon was noted in the study conducted by Nagaral et al. [36] on the characterization of $B_4C$ incorporated into aluminum, as well as in the research by Atuanya and Aigbodion [24] on aluminum reinforced with bean pond ash particles.

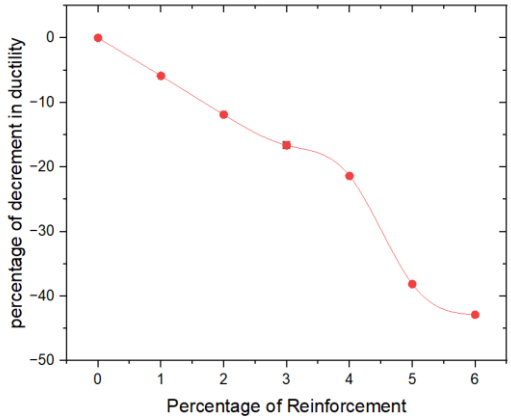


**Fig. 20**. Effect of reinforcement on ductility of Al-Cu-Mg alloy composites

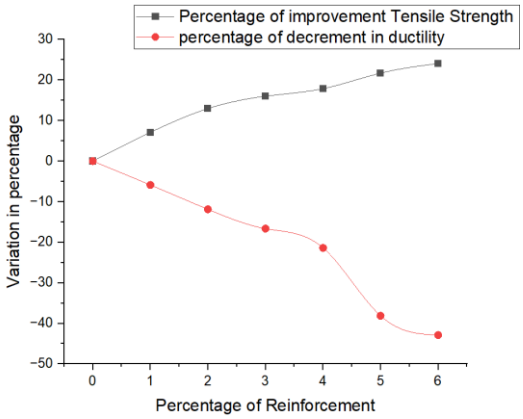


**Fig. 21**. Percentage of Variation of ductility of Al-Cu-Mg alloy and composites

### 3.5 Compression Strength

The influence of 3-µm-sized PSSA particles on the compression strength of the Al-Cu-Mg alloy is illustrated in Fig. 22 a) compression strength and Fig. 22 b) percentage of improvement in compression strength. The plot shows that the compression strength improved when reinforcement was added, from 1% to 6%. The compression strength of Al-Cu-Mg alloy is measured as 238.63 MPa, and it is 317.2 MPa with 6 Wt.% PSSA reinforced composite. 32.93% improvement was recorded when the alloy was added with 6% PSSA reinforcement.

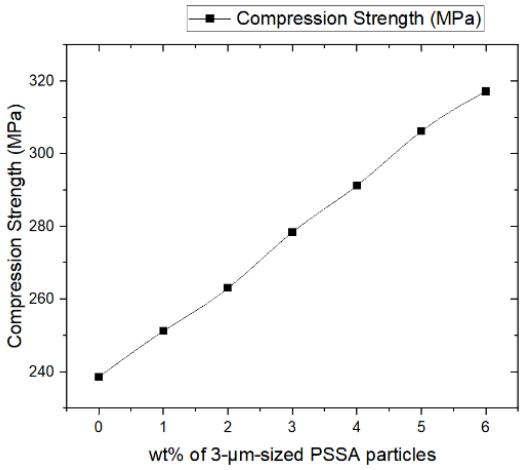


a)

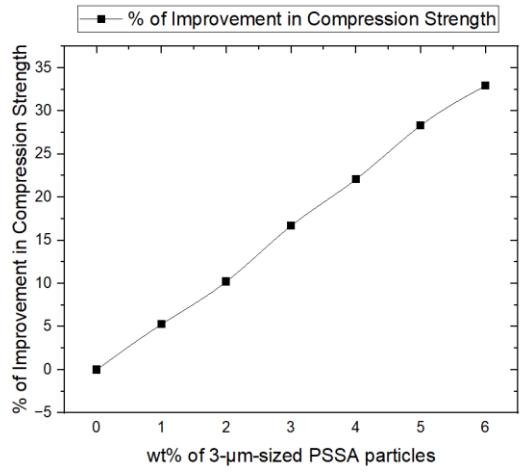


b)

**Fig. 22.** a) Effect of PSSA particles on Compression strength of Al-Cu-Mg alloy; b) Percentage of improvement in compression strength w.r.t. PSSA particles

The improvement of compression strength in aluminum alloy reinforced with ceramic ash (PSSA) can be attributed to the fact that ceramic ash is often characterized by high stiffness and rigidity. When incorporated into aluminum alloy, it reinforces the matrix and increases the overall stiffness of the composite [15, 20]. This results in improved resistance to compression forces. In other ways, reinforcement particles have harder surfaces, and particle movement in between matrices is crucial, constraining dislocation movements and improving the load-bearing capacity of the composites [36]. The results obtained from the current study reveal consistent outcomes in terms of the enhancements observed in both tensile and compressive strengths of the fabricated composites as the number of ceramic particulates added to the alloy increases.

### 3.6 Fractography of Tensile

Fig. 23 illustrates the surface morphology of the Al-Cu-Mg alloy and reinforced composites added with 5 Wt.% and 6 Wt.% of PSSA particles.

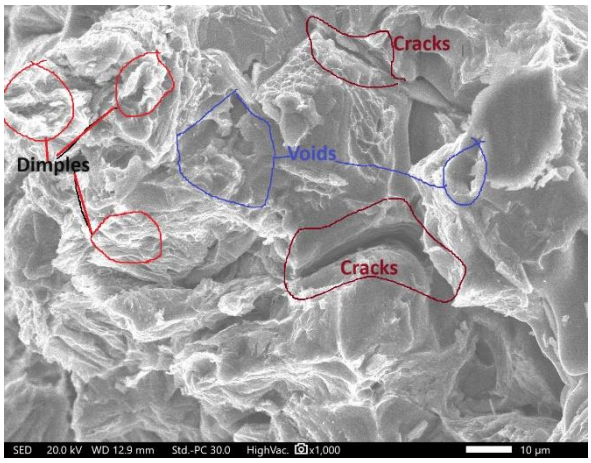


a)

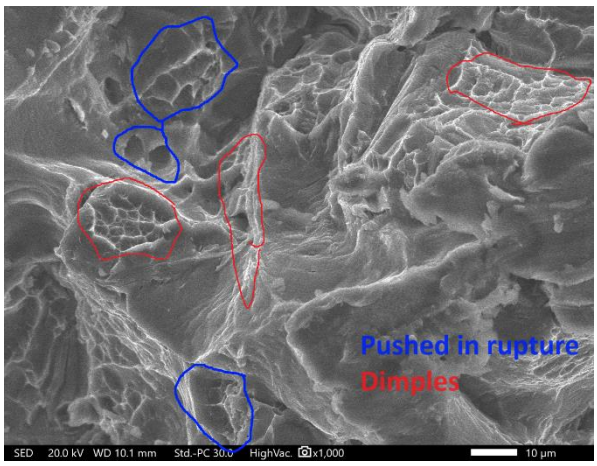


b)

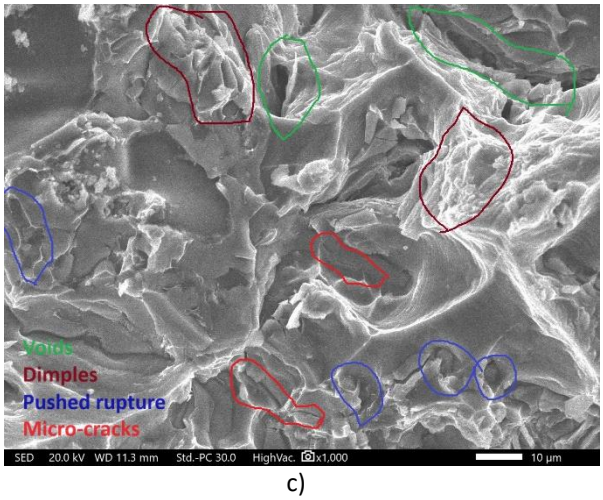


c)

**Fig. 23.** Tensile fracture surface morphology of a) the Al-Cu-Mg alloy; b) the alloy added with the 5 Wt.% of particles and; c) the alloy added with 6 Wt.% of PSSA particles

In Fig. 23 a), the fracture morphology of the alloy is depicted, revealing a plastic fracture morphology. On the other hand, Fig. 23 b) and c) exhibit the fracture profiles of the alloy with the incorporation of 5 Wt.% and 6 Wt.% of PSSA particles. The introduction of these rigid particles alters the size and depth of the dimples in the fractured specimens of the composites, resulting in a brittle fracture morphology due to the presence of PSSA inclusions. Furthermore, cracks are observed to propagate within the rupture, and sharp facets are visible in both composite morphologies. As the mass fractions of PSSA particles in the alloy increase, the matrix material undergoes a brittle fracture as a consequence of the increasing percentage of PSSA particulate content in the matrix. It is obvious that Fig 23 c) has a more brittle zone in comparison with Fig 23 b). In their study, (Kumar et al.) [41] conducted investigations on AZ31D specimens reinforced with SiC particles to examine the presence of microcracks near the fracture surface. They found that the majority of the microvoids were located at the interface of second-stage particles. In one more work, (Nagaral et al.) [36] observed that as the mass fractions of carbide particles in the Al2024 alloy increased, the matrix material exhibited a brittle fracture. This was attributed to the rising percentage of B4C particulate content in the matrix.

### 3.7 Hardness

Figs. 24 a) and b) show the effect of 3-µm-sized PSSA particles on the hardness of the Al-Cu-Mg alloy. The figures illustrate that the hardness of the Al-Cu-Mg alloy improves as the weight percentage of PSSA particles increases from 1 to 6. The alloy's hardness is 126 HV, and the inclusion of 1 Wt.% PSSA particles measured 134 HV. Further, it was raised to 143.5 HV for composites reinforced with 6 Wt. % PSSA.

The improvement in hardness is due to the inclusion of more hard ceramic particles in the soft aluminium matrix. Concerning the strengthening behavior of the composites, the addition of particles to the matrix alloy results in an augmentation of strain energy at the periphery of the particles within the matrix. These tendencies can be attributed to the formation of dislocations at the boundary of the ceramic particles, which is caused by the disparity in thermo-expansion coefficients between the matrix and ceramic particles [12,42].

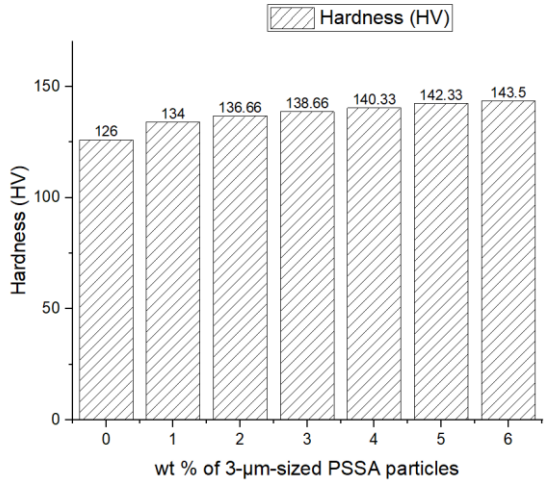


a)

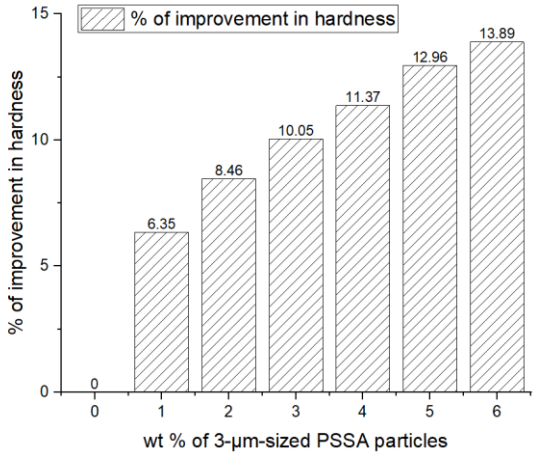


b)

**Fig. 24.** a) Effect of PSSA particles on hardness of Al-Cu-Mg alloy; b) Percentage of improvement in hardness w.r.t. to PSSA particles

### 3.8 Impact Strength

The Impact behavior of reinforced and unreinforced composites has been plotted; Figs. 25 a) and b) specify the specific impact strength and percentage of improvement, respectively. The plot illustrated the effect of PSSA reinforcement on the specific impact strength of Al-Cu-Mg; the effect is very minimal.

The impact strength of the Al-Cu-Al alloy is found to be 2.6 J/mm$^2$. It was found to be 2.589 J/mm$^2$ upon the inclusion of 1 Wt.% PSSA particles. Further, it decreased to 2.575 J/mm$^2$ for 6 Wt.% PSSA, and at this percentage, the maximum decrease was measured as 0.96%. The elastic behaviour of the composite proportionally decreased with the addition of reinforcement because of the lower ratio of matrix and reinforcement, which decreases the energy absorption under an impact load. On the contrary, energy absorption was more or less stable in this study. The 3-µm-sized PSSA particles helped in providing a large surface between the matrix and the particle interface, which helped in the maintenance of impact energy. Fig. 13 a) (SEM images) shows the surface interface between matrix and PSSA particles. Similar observations have been made by (Atuanya and Aigbodion 2014) in their research on Al-Cu-Mg/ bean pod ash synthesis.

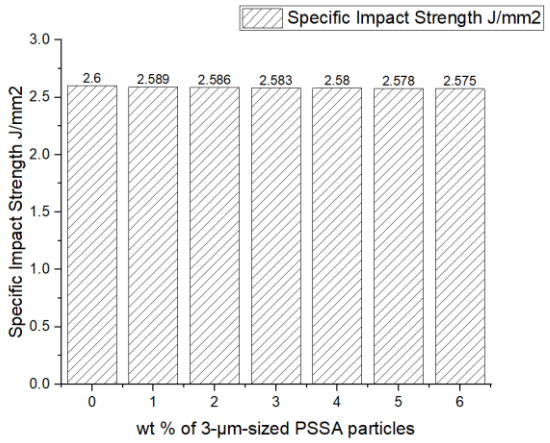


a)

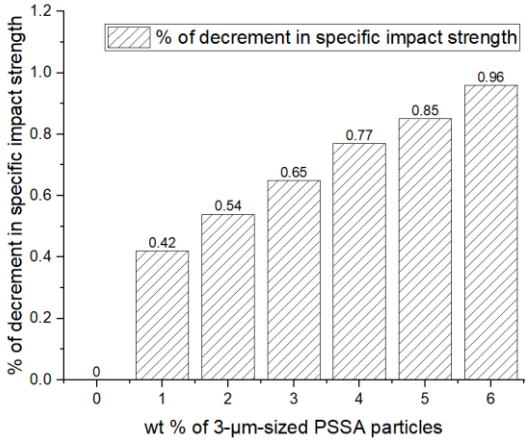


b)

**Fig. 25.** a) Effect of PSSA particles on impact strength of Al-Cu-Mg alloy; b) Percentage of improvement in impact strength w.r.t. to PSSA particles

### 3.9 Wear Analysis

The impact of 3-µm-sized PSSA particles on the wear behavior of the Al-Cu-Mg alloy is illustrated in Fig. 26. Fig. 26 a) illustrates a significant relationship between the weight percentage of PSSA in the Al-Cu-Mg alloy and the wear loss of the compounds. It is evident that as the weight percentage of PSSA increases, the wear loss decreases. This phenomenon can be attributed to the high hardness of the carbides and ceramic ($SiO_2$, $Al2O_3$, and C) particulates found in the PSSA-reinforced composites. These hard ceramic particulates serve as a barrier, effectively preventing wear. Moreover,

the presence of these particles introduces resistance during the dry sliding wear process. A similar observation was made by (Gladstone et al.) [19] in the research work 'Dry sliding wear behavior of AA6061 aluminum alloy composites reinforced rice husk ash particulates'. Another work was recorded by (Nagaral et al.) [36] with Al2024 and boron carbide reinforcements.

Essentially, the impact of the PSSA on Load is a crucial factor that holds great significance in the context of wear loss. In order to examine the impact of load on wear, graphical representations have been created to depict the wear loss in relation to the wear rate under varying loads of 10, 30, 50, and 70 N. These experiments were conducted at a fixed distance of 3768 m and a sliding velocity of 3.14 m/s. Fig. 26 b) illustrates the impact of the applied normal load on the wear characteristics of both the Al-Cu-Mg alloy and composites. The graph reveals that as the load increases from 10 to 70 N, there is a corresponding increase in wear for both the as-cast alloy and the processed composites. At the maximum load of 70 N, the temperature of the sliding face rises. Consequently, as the load on the pin intensifies, there is also a simultaneous escalation in the wear loss of the matrix alloy. This trend is similarly observed in the composites. Notably, the wear loss of the as-cast Al-Cu-Mg alloy is the highest among all the loading conditions.

The wear misfortune in relation to speed variation is graphically represented in Fig. 26 c). The experimental procedure involved adjusting the disc speed between 0.88 and 3.14 m/s while maintaining a constant load of 70 N. The results presented in it indicate that wear misfortune escalates as the disc speed increases. Notably, the impact of sliding velocity on the Al-Cu-Mg alloy surpasses that of PSSA-strengthened metal composites [30,19]. Furthermore, an increase in the sliding speed and load was found to result in a proportional rise in the wear rate, displaying an almost linear trend. Additionally, it was observed that when the composite material is subjected to higher loads, dynamic recrystallization occurs as a consequence of plastic deformation [36]. The findings of this investigation reveal that the composites exhibit a considerably reduced wear loss compared to the Al-Cu-Mg alloy at various sliding speeds. Finally, as the PSSA particulates increase, the wear losses of the composite decrease. These outcomes are consistent with prior investigations conducted by other researchers, reinforcing with similar type ceramic reinforcements $B_4C$ and $CaCo_3$ [36,37].

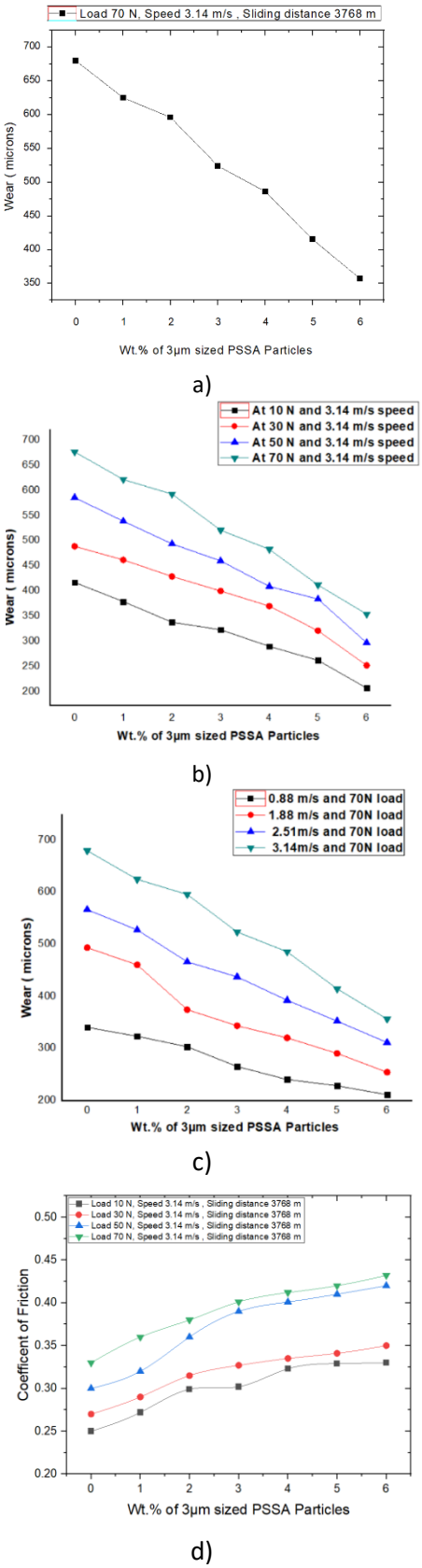


**Fig. 26**. a) Wear (microns) of Al-Cu-Mg alloy reinforced with varying Wt.% of PSSA particulates; b) Wear (microns) of alloy and its PSSA composites at constant speed and varying loads; c) Wear (microns) of Al-Cu-Mg alloy and its PSSA composites at constant load and varying speeds; d) Variation in coefficient of friction with varying weight percentages of PSSA.

Further, the friction behavior of Al-Cu-Mg alloy and composites with PSSA was analyzed by studying the changes in the coefficient of friction during dry sliding wear tests under various loads, as illustrated in Fig. 26 d). During the starting period of the dry sliding test, the friction force initially increases and then fluctuates around a mean value. To determine this mean value, the individual friction coefficients are analyzed, excluding the initial rising phase. Notably, the mean coefficient of friction has been observed to increase with an increasing load for both the Al-Cu-Mg alloy and the composites containing PSSA. Further, Fig. 26 d) demonstrated that when the load is higher, the frictional force rises due to increased dissipation of energy, resulting in a higher temperature at the contact point. Consequently, the coefficient of friction also rises with the increasing load. Further, the coefficient of friction increases with a higher PSSA content in the composite. This is unexpected because these particles are expected to form weak connections with the roughness of the counter face due to their low oxide-metal interfacial energy. Additionally, they contribute to forming a thicker transfer layer, which should further weaken the connections. Hence, the only logical conclusion is that the plowing of the sliding surface and micro-cutting during three-body wear are responsible for the heightened frictional forces in composites that contain a greater amount of hard oxide particles. A similar finding was made by Apasia et al. [43]. In their study, they investigated the wear behavior of Al-Si-Fe Alloy/Coconut Shell Ash Particulate Composites.

### 3.10 SEM Analysis on Worn Morphology

It is important to analyze the worn-out surface of Al-Cu-Mg alloy and Al-Cu-Mg alloy added with 6 Wt.% of PSSA particles. Fig. 27 a) and b) display the scanning electron microscopy (at 1000X) images of the worn-out surface of Al-Cu-Mg alloy and composite added with 6 Wt.% of PSSA respectively were tested at 70 kN load, 3.14 m/s speed, and 3768 m sliding distance. Fig. 28 a) and b) illustrate the same specimens' micrographs at 2000X magnification. When Al-Cu-Mg alloy material is subjected to sliding on a disc, the alloy exhibits lower hardness compared to the material of the rubbing disk, resulting in the viscous flow of the Al-Cu-Mg matrix. This flow takes the form of a pin, leading to plastic deformation of the surface of the specimen and a significant amount of material being lost. Fig. 27 a) and Fig. 28 a) reveal the existence of grooves, micro-pits, and a delaminated/ fractured layer. These surface characteristics are likely to have contributed to the observed increase in wear loss.

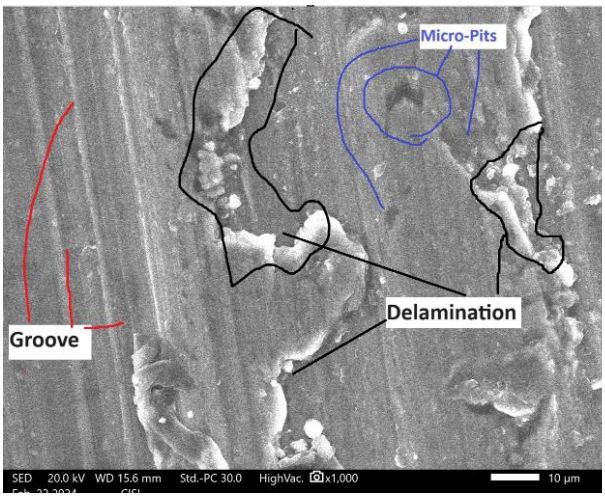


a)

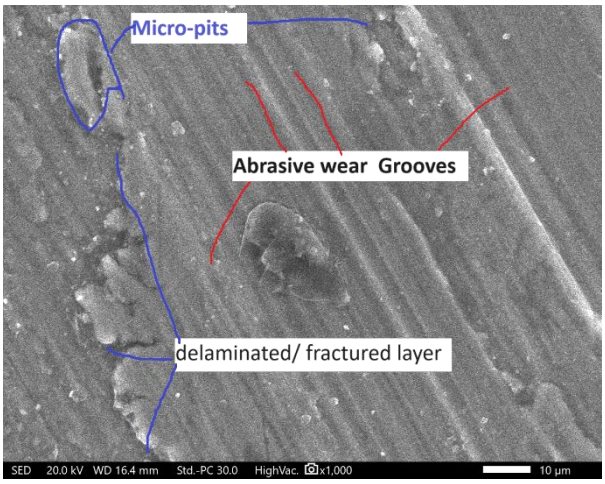


b)

**Fig. 27.** SEM (1000X magnification) images of worn-out surfaces of (a) Al-Cu-Mg alloy at and (b) Composite added with 6 Wt.% PSSA particles

Fig. 27 b) and Fig. 28 b) demonstrate that the inclusion of 6 Wt.% PSSA particles in the Al-Cu-Mg alloy restricts the matrix's viscous flow. The addition of PSSA particles leads to a decrease in grooves and erosion, indicating an enhanced resistance to wear loss [36,38,43]. Moreover, the stress appears to be transferred to the hard particles, resulting in strain concentration around these particles. Consequently, the presence of these hard particles contributes to a reduction in cracks and grooves on the worn surface area.

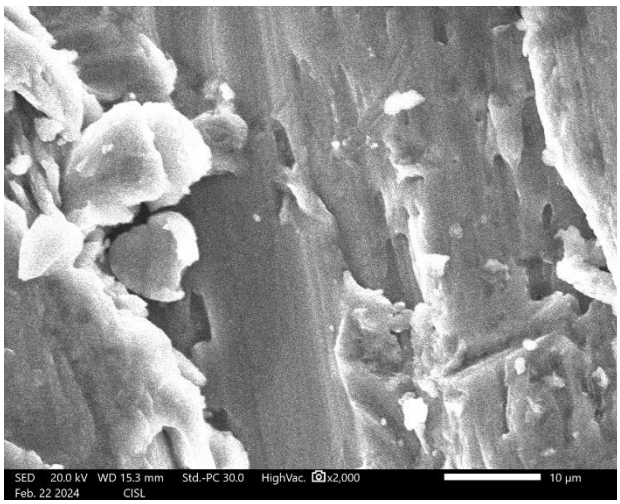


a)

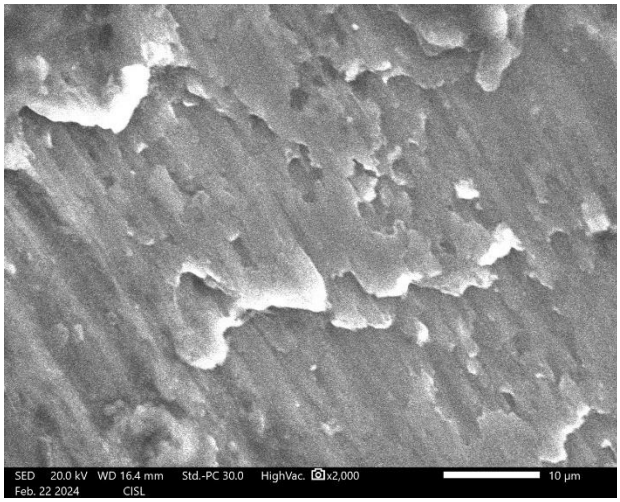


b)

**Fig. 28.** SEM (2000X magnification) images of worn-out surfaces of a) Al-Cu-Mg alloy; b) Composite added with 6 Wt.% PSSA particles

## 4. CONCLUSION

The Al-Cu-Mg alloys reinforced with varying contents of 3-µm-sized palm sprout shell ash (PSSA) have been successfully made by the ultrasonic-assisted stir casting process. The microstructural, density, hardness, tensile, compression, impact, and wear behavior of composites were studied. The following observations were made:

- Micrographs obtained using an optical metallurgical microscope and a scanning electron microscope demonstrate that the Al-Cu-Mg alloy exhibits a homogeneous dispersion of PSSA particles. The presence of PSSA particles in the prepared composites was confirmed through EDS and XRD analysis.
- Incorporating PSSA reinforcement has led to enhancements in hardness, compression strength, tensile strength. The hardness, ultimate tensile strength, and compression strength were improved by 13.89%, 24.04%, and 32.93%, respectively, with the 6 Wt.% PSSA-reinforced composite.
- The addition of reinforcement—in this work, the composite reinforced with 6% PSSA particles showed the highest decrease, 42.87%—has reduced the ductility of the Al-Cu-Mg alloy composite.
- PSSA particles have a positive effect; the decrement of impact strength is minimal. The maximum decrement was observed at 0.96% with the 6 Wt.% PSSA-reinforced composite.
- The fractured surfaces observed in tensile tests indicate the occurrence of both ductile and brittle fracture mechanisms. As the reinforcement percentage increases, the brittle fracture is more evident.
- The wear resistance of the Al-Cu-Mg alloy has been found to increase with the inclusion of 3-µm-sized PSSA particles. The applied load and sliding speed influence the wear behavior of the alloy and its composites. As the speed and load increase, the wear rate and coefficient of friction of both the alloy and its composites reinforce the coefficient of friction of both the alloy and its composites, and the coefficient of friction of both the alloy and its composites reinforced with PSSA particles also increases. However, the incorporation of PSSA reinforcement leads to an overall improvement in wear resistance.

### Conflicts of Interest

The authors declare no conflict of interest.

## REFERENCES

[1] A.K. Sharma, R. Bhandari, A. Aherwar, C. Pinca-Bretotean, A study of fabrication methods of aluminium based composites focused on stir casting process. *Materials Today: Proceedings*, 27, 2020: 1608–1612. https://doi.org/10.1016/j.matpr.2020.03.316

[2] M.K. Surappa, Aluminium matrix composites: Challenges and opportunities. *Sadhana*, 28, 2003: 319–334. https://doi.org/10.1007/bf02717141

[3] M.M. Alam, B.S Motgi, Study on Microstructure and Mechanical Properties of Al7068 Reinforced with Silicon Carbide and Fly Ash by Powder Metallurgy. *International Journal for Modern Trends in Science and Technology, 7*(09), *2021*: 47–53.

https://doi.org/10.46501/ijmtst0709009

[4] G. Moona, R.S. Walia, V. Rastogi, R. Sharma, Aluminium metal matrix composites: A retrospective investigation. *Indian Journal of Pure & Applied Physics, 56,* 2017, 164–175.

[5] G.J.N. Gladson, K.D. Raj, R. Devesh, R.J. Prakash, S. Pandurangan, Performance analysis and mechanical behavior of aluminum metal matrix composite. *Journal of Physics: Conference Series*, 2484, 2023: 012027. https://doi.org/10.1088/1742-6596/2484/1/012027

[6] M.A. Maleque, A. Atiqah, R.J. Talib, H. Zahurin. New natural fibre reinforced aluminium composite for automotive brake pad. *International Journal of Mechanical and Materials Engineering (IJMME)*, 7(2), 2012: 166–170.

[7] V.S Aigbodion, Bean pod ash nanoparticles a promising reinforcement for aluminium matrix biocomposites. *Journal of Materials Research and Technology*, 8(6), 2019: 6011–6020. https://doi.org/10.1016/j.jmrt.2019.09.075

[8] A. Bahrami, N. Soltani, M.I. Pech-Canul, C.A. Gutiérrez, Development of metal-matrix composites from industrial/agricultural waste materials and their derivatives. *Critical Reviews in Environmental Science and Technology*, 46(2), 2016: 143–208. https://doi.org/10.1080/10643389.2015.1077067

[9] L. Lancaster, M.H. Lung, D. Sujan. Utilization of Agro-Industrial Waste in Metal Matrix Composites: Towards Sustainability. *International Journal of Environmental, Ecological, Geomatics, Earth Science and Engineering*, 7(1), 2013: 25-33.

[10] S.P. Dwivedi, A. Saxena, A. Kumaraswamy, R. Sahu, Synthesis and characterisation of waste SAC- and RHA-reinforced aluminium-based composite. *Green Materials*, 10(1), 2022: 23–34. https://doi.org/10.1680/jgrma.20.00042

[11] S. Das, T.K. Dan, S.V. Prasad, P.K. Rohatgi, Aluminium alloy—rice husk ash particle composites. *Journal of Materials Science Letters*, 5, 1986: 562–564. https://doi.org/10.1007/bf01728691

[12] D. Siddharth, J.B. Rao, Synthesis & Characterization of Rha (Rice Husk Ash) Particulates Reinforced A7075 Composites. *International Journal of Advances in Mechanical and Civil Engineering*, 4(3), 2017: 105–111.

[13] M. Safiuddin, Z.J. Mohd, M.A. Salam, M.S. Islam, R. Hashim, Utilization of solid wastes in construction materials. *International Journal of the Physical Sciences*, 5(13), 2010: 1952–1963.

[14] K.K Alaneme, H.I. Eze, M.O Bodunrin, Corrosion behaviour of groundnut shell ash and silicon carbide hybrid reinforced Al-Mg-Si alloy matrix composites in 3.5% NaCl and 0.3M $H_2SO_4$ solutions. *Leonardo Electronic Journal of Practices and Technologies*, (2), 2015: 129-146.

[15] K.K. Alaneme, M.O. Bodunrin, A.A. Awe, Microstructure, mechanical and fracture properties of groundnut shell ash and silicon carbide dispersion strengthened aluminium matrix composites. *Journal of King Saud University - Engineering Sciences*, 30(1), 2018: 96–103. https://doi.org/10.1016/j.jksues.2016.01.001

[16] M. Poornesh, J.X. Saldanha, J. Singh, G.M. Pinto, Gaurav, Comparison of Mechanical Properties of Coconut Shell Ash and SiC Reinforced Hybrid Aluminium Metal Matrix Composites. *American Journal of Materials Science*, 7(4), 2017: 116-119.

[17] M. Abdulwahab, O. Umaru, M. Bawa, H.A. Jibo, Microstructural and thermal study of Al-Si-Mg/melon shell ash particulate composite. *Results in Physics*, 7, 2017: 947–954. https://doi.org/10.1016/j.rinp.2017.02.016

[18] I. Dinaharan, K. Kalaiselvan, N. Murugan, Influence of rice husk ash particles on microstructure and tensile behavior of AA6061 aluminum matrix composites produced using friction stir processing. *Composites Communications*, 3, 2017: 42–46. https://doi.org/10.1016/j.coco.2017.02.001

[19] J.A.K. Gladston, I. Dinaharan, N.M. Sheriff, J.D.R. Selvam, Dry sliding wear behavior of AA6061 aluminum alloy composites reinforced rice husk ash particulates produced using compocasting. *Journal of Asian Ceramic Societies*, 5(2), 2017: 127–135. https://doi.org/10.1016/j.jascer.2017.03.005

[20] J.A.K. Gladston, N.M. Sheriff, I. Dinaharan, J.D.R. Selvam, Production and characterization of rich husk ash particulate reinforced AA6061 aluminum alloy composites by compocasting. *Transactions of Nonferrous Metals Society of China*, 25(3), 2015: 683–691. https://doi.org/10.1016/s1003-6326(15)63653-6

[21] O.O. Joseph, K.O. Babaremu, Agricultural Waste as a Reinforcement Particulate for Aluminum Metal Matrix Composite (AMMCs): A Review. *Fibers*, 7(4), 2019: 33. https://doi.org/10.3390/fib7040033

[22] P. Mangalore, C.S. Vittal, Akash, A. Ulvekar, Abhiram, J. Sanjay, Advaith, Study of tribological properties of Al 7079 alloy reinforced with agro waste particles. *AIP Conference Proceedings*, 2080(1), 2019: 020015. https://doi.org/10.1063/1.5092898

[23] P.B. Madakson, D.S.Yawas, A. Apasi. (2022). Characterization of Coconut Shell Ash for Potential Utilization in Metal Matrix Composites for Automotive Applications. *International Journal of Engineering Science and Technology (IJEST)*, *4*(0975–5462), 1190–1198.

[24] C.U. Atuanya, V.S. Aigbodion, Evaluation of Al–Cu–Mg alloy/bean pod ash nanoparticles synthesis by double layer feeding–stir casting method. *Journal of Alloys and Compounds*, 601, 2014: 251–259. https://doi.org/10.1016/j.jallcom.2014.02.086

[25] B. Parveez, M.A. Maleque, N.A. Jamal, Influence of agro-based reinforcements on the properties of aluminum matrix composites: a systematic review. *Journal of Materials Science*, 56, 2021: 16195–16222. https://doi.org/10.1007/s10853-021-06305-2

[26] D. Dhaneswara, J.F. Fatriansyah, M.R. Firmansyah, Effect of addition of sodium chloride in sodium nitrate-sodium fluoride-based degasser in aluminum casting. *IOP Conference Series: Materials Science and Engineering*, 578, 2019: 012066. https://doi.org/10.1088/1757-899x/578/1/012066

[27] T. Triyono, N. Muhayat, A. Supriyanto, L. Lutiyatmi, Effect of Degassing Treatment on the Interfacial Reaction of Molten Aluminum and Solid Steel. *Archives of Foundry Engineering*, 17(2), 2017: 227–239. https://doi.org/10.1515/afe-2017-0080

[28] T. Nagaraju, A.C. Tejaswini, R.P. Babu, An Investigation of Alumina Reinforcement Effect on Mechanical Properties of Al 356 Based Metal Matrix Composite. *International Journal of Latest Engineering Science (IJLES)*, 02(03), 2019: 18–23.

[29] K.K. Alaneme, I.B. Akintunde, P.A. Olubambi, T.M. AdewaleFabrication characteristics and mechanical behaviour of rice husk ash – Alumina reinforced Al-Mg-Si alloy matrix hybrid composites. *Journal of Materials Research and Technology*, 2(1), 2013: 60–67. https://doi.org/10.1016/j.jmrt.2013.03.012

[30] A.R. Reddy, P.V. Krishna, R.N. Rao, Two-body abrasive wear behaviour of AA6061-2SiC-2Gr hybrid nanocomposite fabricated through ultrasonically assisted stir casting. *Journal of Composite Materials*, 53(15), 2019: 2165–2180. https://doi.org/10.1177/0021998318822723

[31] Z. Liu, Q. Han, J. Li, Ultrasound assisted in situ technique for the synthesis of particulate reinforced aluminum matrix composites. *Composites Part B: Engineering*, 42(7), 2011: 2080–2084. https://doi.org/10.1016/j.compositesb.2011.04.004

[32] A.P. Reddy, P.V. Krishna, R.N. Rao, Tribological Behaviour of Al6061–2SiC-xGr Hybrid Metal Matrix Nanocomposites Fabricated through Ultrasonically Assisted Stir Casting Technique. *Silicon*, 11, 2019: 2853–2871. https://doi.org/10.1007/s12633-019-0072-9

[33] Y. Yang, Z. Liu, R. Jiang, R Li, X. Li, Microstructural evolution and mechanical properties of the AA2219/TiC nanocomposite manufactured by ultrasonic solidification. *Journal of Alloys and Compounds*, 811, 2019: 151991. https://doi.org/10.1016/j.jallcom.2019.151991

[34] P. Ajagol, B.N. Anjan, R.N. Marigoudar, G.V.P. Kumar, Effect of SiC Reinforcement on Microstructure and Mechanical Properties of Aluminum Metal Matrix Composite. *IOP Conference Series: Materials Science and Engineering*, 376, 2018: 012057. https://doi.org/10.1088/1757-899x/376/1/012057

[35] B. Malomo, O. Fadodun, K. Oluwasegun, A. Ogunbodede, S. Ibitoye, L. Adekoya, On the solidification characteristics and mechanical properties of aluminum alloy AA 6061/$Al_2O_3$-SICp composite produced by high pressure die casting, *Journal of Engineering Science and Technology*, 12(7), 2017: 1804–1818.

[36] M. Nagaral, R.G. Deshapande, V. Auradi, S.B. Boppana, S Dayanand, M.R. Anilkumar, Mechanical and Wear Characterization of Ceramic Boron Carbide-Reinforced Al2024 Alloy Metal Composites. *Journal of Bio-and Tribo-Corrosion*, 7(1), 2021: 19.

https://doi.org/10.1007/s40735-020-00454-8

[37] M.S. Prabhu, A.E. Perumal, S. Arulvel, R.F. Issac, Friction and wear measurements of friction stir processed aluminium alloy 6082/$CaCO_3$ composite. *Measurement*, 142, 2019: 10–20. https://doi.org/10.1016/j.measurement.2019.04.061

[38] N.S. Prabhakar, N. Radhika, R. Raghu, Analysis of Tribological Behavior of Aluminium/$B_4C$ Composite Under Dry Sliding Motion. *Procedia Engineering*, 97, 2014: 994–1003. https://doi.org/10.1016/j.proeng.2014.12.376

[39] P. Ajagol, B.N. Anjan, R.N. Marigoudar, G.V.P. Kumar, Effect of SiC Reinforcement on Microstructure and Mechanical Properties of Aluminum Metal Matrix Composite. *IOP Conference Series: Materials Science and Engineering*, 376, 2018: 012057. https://doi.org/10.1088/1757-899x/376/1/012057

[40] P. Poddar, S. Mukherjee, K. Sahoo, The Microstructure and Mechanical Properties of SiC Reinforced Magnesium Based Composites by Rheocasting Process. *Journal of Materials Engineering and Performance*, 18, 2009: 849–855. https://doi.org/10.1007/s11665-008-9334-1

[41] K.C.K. Kumar, B.R. Kumar, N.M. Rao, Microstructural, Mechanical Characterization, and Fractography of AZ31/SiC Reinforced Composites by Stir Casting Method. *Silicon*, 14(9), 2022: 5017–5027. https://doi.org/10.1007/s12633-021-01180-7

[42] L. Fischer, Literature survey report: nano-dispersion strengthening of aluminium, *Introduction to Research. University of Colorado*, Boulder, USA, 2004.

[43] A. Apasi, P.B. Madakson, D.S. Yawas, and V.S. Aigbodion, Wear Behaviour of Al-Si-Fe Alloy/Coconut Shell Ash Particulate Composites. *Tribology in Industry*, 3(1), 2012: 36–43.